Development of a virtual metrology method using plasma harmonics analysis

H. Jun, J. Shin, S. Kim, and H. Choi

Citation: AIP Advances **7**, 075205 (2017); doi: 10.1063/1.4993282
View online: http://dx.doi.org/10.1063/1.4993282
View Table of Contents: http://aip.scitation.org/toc/adv/7/7
Published by the American Institute of Physics

Development of a virtual metrology method using plasma harmonics analysis

H. Jun,[a] J. Shin, S. Kim, and H. Choi
Semiconductor Equipment Technology Team, Advanced Technology Lab., LG Electronics, 222 LG-ro Jinwi-myeon, Pyeongtaek-si, Gyeonggi-do 17709, Republic of Korea

(Received 28 January 2017; accepted 28 June 2017; published online 12 July 2017)

A virtual metrology technique based on plasma harmonics is developed for predicting semiconductor processes. From a plasma process performed by 300 mm photoresist stripper equipment, a strong correlation is found between optical plasma harmonics intensities and the process results, such as the photoresist strip rate and strip non-uniformity. Based on this finding, a general process prediction model is developed. The developed virtual metrology model shows that the *R*-squared (R^2) values between the measured and predicted process results are 95% and 64% for the photoresist strip rate and photoresist strip non-uniformity, respectively. This is the first research on process prediction based on optical plasma harmonics analysis, and the results can be applied to semiconductor processes such as dry etching and plasma enhanced chemical vapor deposition. [http://dx.doi.org/10.1063/1.4993282]

I. INTRODUCTION

Semiconductor process inspection has become an increasingly important issue with the development of 10 nm semiconductor manufacturing process technology. For critical dimension (*CD*) inspection, the scanning electron microscope (*SEM*) and transmission electron microscope (*TEM*) have been mainly used. For the past few decades, these types of inspection techniques have been successfully applied to semiconductor processes, becoming essential tools for measuring the critical dimensions of semiconductor devices. Process metrology is actively applied in the manufacturing of dynamic random access memory (*DRAM*) and 3-dimensional *NAND* flash memory with an increasing importance. As recent developments call for semiconductor devices with sizes less than 10 nm, new technologies are being developed to complement inspection tools such as *SEM* and *TEM*, and process virtual metrology is emerging as one of the most promising techniques. Process virtual metrology[1–4] is a means for predicting process results and device yield using the sensor data from the process equipment and is appropriate for maintaining mass production lines. In order to apply process virtual metrology, an algorithm is needed to select effective physical factors of the semiconductor equipment and to convert complex data into measured process results. Until now, mass production process has been maintained using equipment sensor values, and wafer process results were not directly calculated by the process monitoring data from the plasma reactor. In comparison, the purpose of virtual metrology is to directly predict process results and device yield trends according to the variations in plasma reactor conditions. To achieve this, various advanced mathematical regression methods have been used in the virtual metrology of semiconductor processes,[5–8] and a metrology noise reduction algorithm has been recently developed for detecting and classifying process faults.[9] In more advanced approaches, wafer-to-wafer process controls based on virtual metrology is tested for chemical and mechanical planarization processes.[10] In addition, a study was conducted to enhance virtual metrology using the electron energy distribution function in the dry etch plasma reactor.[11]

[a]Electronic mail address: mtsconst@kaist.ac.kr

In this paper, a virtual metrology technique based on plasma harmonics[12,13] is developed for predicting semiconductor processes. By analyzing the *R*-squared (R^2) value[14] between measured wafer process results and plasma's optical harmonics data, it is found that final wafer process results have strong correlations with the intensity signals of measured optical plasma harmonics. Using this correlation, a mathematical model capable of predicting measured wafer process results is developed. The analytical results of the model show that the *R*-squared values of the virtual inspection results are 95% for the photoresist strip rate, and 64% for photoresist strip non-uniformity. This study is the first experimental research that converts measured optical plasma harmonics data into measured wafer process results, and a mathematical model for analyzing processes is quantitatively developed.

II. DIAGNOSTICS PRINCIPLE AND MATHEMATICAL MODEL

Plasma harmonics signals are generated by the nonlinear motion rf sheath[15,16] and can be measured using electrical and optical sensors. These harmonics signals are physically related to plasma parameters, including electron temperature, electron density, ion energy distribution, and chemical reaction. According to previous research on plasma harmonics, the local plasma frequency $\omega_{pe}=(n_e e^2/m_e\varepsilon_0)^{1/2}$ interacts with the plasma harmonics of the driving frequency ω_{rf} at $\omega_{pe}=l\times\omega_{rf}$ (l=1, 2, 3...).[17] This plasma parallel resonance generates highly energetic electron beams in bulk plasmas and affects the conduction and displacement currents of bulk plasma.[18,19] Therefore, plasma harmonics contribute toward varying bulk plasma's electrochemical condition. In the case of inductively coupled plasma (*ICP*), nonlinear harmonics are generated by capacitive coupling due to the *ICP* antenna voltage.[20] Because of the high asymmetry ratio effect between *ICP*'s antenna area and the chamber ground area, there exists a high-voltage rf sheath near *ICP* antenna. Although the sheath nonlinearity of *ICP* is not stronger than conventional capacitively coupled plasma (*CCP*), nonlinear signals of up to third or fourth harmonics are regularly found in *ICP*. For this reason, the plasma harmonics frequency can be an optimal indicator for describing plasma's physical characteristics and used to predict plasma processes. To achieve this end, it is necessary to define a new vector space consisting of plasma harmonics intensities:

$$H_{ij}(\tau)=\left(H_{0j}(\tau),H_{1j}(\tau),H_{2j}(\tau),\cdots,H_{nj}(\tau)\right), \tag{1}$$

where indices i and j are the plasma harmonics order and the process inspection order, respectively, and n represents the maximum plasma harmonics order among the plasma harmonics order i. $H_{ij}(\tau)$ represents the harmonics signal intensities in optical plasma emission. $H_{0j}(\tau)$ is defined as the static intensity of the optical plasma emission, $H_{1j}(\tau)$ is the fundamental plasma harmonics intensity, and $H_{ij}(\tau)$ denotes conventional plasma harmonics intensities for higher orders. In general, because plasma harmonics signal intensity is a time-dependent parameter, $H_{ij}(\tau)$ in Eq. (1) can be averaged over the unit wafer process time period $\delta\tau$ and is written as

$$\bar{H}_{ij}=\frac{1}{\delta\tau}\int H_{ij}(\tau)d\tau=\left(\bar{H}_{0j},\bar{H}_{1j},\bar{H}_{2j},\cdots,\bar{H}_{nj}\right). \tag{2}$$

In a similar manner, arbitrary plasma process results measured by inspection tools such as *SEM*, *TEM*, and ellipsometer can be defined as a vector space:

$$CD_{M,j}=(CD_{M,1},CD_{M,2},CD_{M,3},\cdots,CD_{M,k}), \tag{3}$$

where $CD_{M,j}$ is the arbitrary process results measured at inspection order j, and k indicates the sample size of the measured order j. Similarly, virtual $CD_{V,j}$ predicted by the mathematical model can be written as

$$CD_{V,j}=(CD_{V,1},CD_{V,2},CD_{V,3},\cdots,CD_{V,k}). \tag{4}$$

Virtual $CD_{V,j}$ in Eq. (4) can be expressed with a linear combination of average plasma harmonics $H_{ij}(\tau)$:

$$CD_{V,j}\equiv\bar{\alpha}\sum_{i=0}^{i=n}\left|R_i^2\right|\bar{H}_{ij}=\bar{\alpha}\left(\left|R_0^2\right|\bar{H}_{0j}+\left|R_1^2\right|\bar{H}_{1j}+\left|R_2^2\right|\bar{H}_{2j}+\cdots+\left|R_n^2\right|\bar{H}_{nj}\right), \tag{5}$$

where R_i^2 is the statistical R-squared (R^2) value of data pair $\left(\bar{H}_{ij}, CD_{M,j}\right)$ in Eq. (2) and Eq. (3), written as $R_i^2\left(\bar{H}_{ij}, CD_{M,j}\right)$ in this paper. Mathematically, Eq. (5) refers to the distributed function in the basis $\bar{H}_{ij}$ according to the magnitude of R_i^2. Because $R_i^2\left(\bar{H}_{ij}, CD_{M,j}\right)$ is calculated based on the statistical correlation of the inspection range $1 \le j \le k$, the accuracy of the time series in virtual metrology cannot be smaller than the CD sample size k. R_i^2 in Eq. (5) can now be written as

$$R_i^2 = 1 - \frac{SS_{res,i}}{SS_{tot}} = 1 - \frac{\sum_{j=1}^{j=k} \left(CD_{M,j} - CD_{f,ij}\right)^2}{\sum_{j=1}^{j=k} \left(CD_{M,j} - CD_{M,av}\right)^2} \tag{6}$$

$$where \quad CD_{f,ij} = a_i \bar{H}_{ij} + b_i, \quad CD_{M,av} = \frac{1}{k}\sum_{j=1}^{j=k} CD_{M,j}$$

$SS_{\mathrm{res,i}}$ and SS_{tot} denote regression and residual sums of squares, respectively. $CD_{f,ij}$ and $CD_{M,av}$ indicate linearly fitted CD and the average CD in the inspection range $1 \le j \le k$, respectively. Constants a_i and b_i are the slope and the intercept of the linear regression parameters for determining the fitted $CD_{f,ij}$. $\bar{\alpha}$ in Eq. (5) represents a constant determined by measured $CD_{M,j}$, R_i^2 and $\bar{H}_{ij}$:

$$\bar{\alpha} = \frac{1}{k}\sum_{j=0}^{j=k} \alpha_j \text{ , where } \alpha_j = \frac{CD_{M,j}}{\sum_{i=0}^{i=n} \left|R_i^2\right| \bar{H}_{ij}}. \tag{7}$$

Because α_j is the proportional factor between measured $CD_{M,j}$ and $\sum_{i=0}^{i=n}\left|R_i^2\right|\bar{H}_{ij}$, α_j is generated for each inspection j. To obtain a statistically stable α_j for a wide inspection range, it is necessary to average α_j over a specific inspection sample range $0 \le j \le k$. The average value of α_j (i.e. $\bar{\alpha}$) provides a statistically stable proportional factor for predicting $CD_{V,j}$ in Eq. (5). From an empirical point of view, $\bar{\alpha}$ has to be updated periodically according to the variations in the plasma reactor condition, and the frequency of updating can be determined from the amount of plasma reactor's internal part etch or the thickness of the process byproduct on the surfaces of the plasma reactor.

III. EXPERIMENTAL SETUP AND OPTICAL SENSING SYSTEM

Figure 1 represents the 300 mm photoresist stripper system used in plasma virtual metrology. In the photoresist strip process, a driving frequency of ω_{rf}=400 kHz with 5.5 kW is supplied to the ferrite inductively coupled plasma. The quartz reactor is surrounded by the ferrite block with a relative magnetic permeability of μ/μ_0=1300 for magnetic field confinement. The plasma formed by the induced electric field of the external coil is first diffused to the exhaust holes linked to the quartz reactor shown in Fig. 1. The secondary diffusion of the plasma reaches the wafer region through the lower quartz gas baffle. Process conditions, including gas pressure of 0.8 Torr, mixed gas flow rate O_2 of 12.0 *LPM*, and N_2=1.2 *LPM*, are applied for the photoresist strip. During the photoresist strip process, the temperature of the dot-chuck station is set at 240°C and an *I*-line (wavelength 365 nm) photoresist with a 3.5 um thickness[21] is used. The total plasma process time is limited to 10 seconds. The plasma diagnostics system for measuring plasma optical emission is directly connected to the chamber view port, which is located 12 mm above the surface of the dot-chuck station.

Figure 2 shows the sensor system used for measuring plasma optical emission. The plasma optical emission spectrum from the plasma reactor is gathered by a high-speed photodiode, which has an absorption wavelength range of 320-1200 nm and a response time resolution of 1 GHz. The electric signals measured at the photodiode is transferred through an operational amplifier, analog-digital converter (125 MHz sampling rate), and field programmable gate array (*FPGA*). After processing the signals, the analysis computer indicated a time resolution of 8 nanoseconds. For measuring the photoresist strip rate and strip non-uniformity, *Woollam M2000V* ellipsometer[22] is used with 49-point

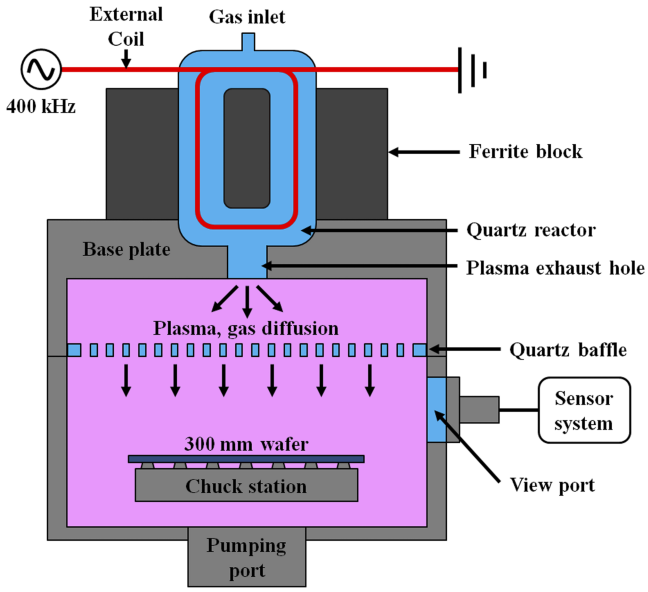

FIG. 1. Experimental setup of the photoresist stripper system for the 300 mm wafer process.

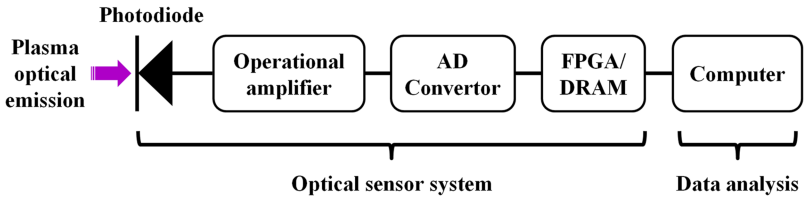

FIG. 2. Schematic diagram of the optical diagnostics system for measuring plasma harmonics signals.

inspection. For $CD_{V,j}$ prediction, results from eight wafer processes and optical plasma harmonics measurements are applied.

IV. EXPERIMENTAL RESULTS AND DATA ANALYSIS

Figures 3(a) and 3(b) show the measured plasma optical emission signal in time domain and its fast Fourier transformation (*FFT*) results, respectively. Because the time domain signal in Fig. 3(a) is the optical intensity (i.e. amplitude), which measures the bulk plasma zone, there are two optical peak intensities within a single sinusoidal wave of 400 kHz (2.5 μs). Therefore, all optical harmonics intensity peaks in frequency domain appeared at twice the rf driving frequency of 400 kHz. The measured plasma harmonics intensity peaks H_0 (0 MHz), H_1 (0.8 MHz), H_2 (1.6 MHz), and H_3 (2.4 MHz) in Fig. 3(b) support this interpretation. In addition, the plasma harmonics signal over H_3 (2.4 MHz) is not detected in the *FFT* spectrum data. Table I presents average harmonics intensities $\bar{H}_{ij}$, average strip rate (*ASR*), and strip non-uniformity (*SNU*) measured by the photodiode sensor and the ellipsometer. Table II shows the *R*-squared values calculated using Table I and Eq. (6). With the results, $\bar{\alpha}$ can be determined from Eq. (7).

Figures 4(a) and 4(b) show predicted photoresist strip rates and photoresist strip non-uniformities, respectively. A wafer inspection range of $1 \le j \le 4$ is used to calculate $\bar{\alpha}$, and the determined $\bar{\alpha}$ is applied to Eq. (5) to predict $CD_{V,j}$ for $1 \le j \le 8$. The calculation results show that $R^2(CD_{M,j}, CD_{V,j}) \approx 95\%$ for the average photoresist strip rate in Fig. 4(a), and $R^2(CD_{M,j}, CD_{V,j}) \approx 64\%$ for photoresist strip non-uniformity in Fig. 4(b). Comparing the virtual metrology results of Fig. 4(a) and Fig. 4(b), $R^2(CD_{M,j}, CD_{V,j})$ of the average photoresist strip rate is higher than $R^2(CD_{M,j}, CD_{V,j})$ of photoresist strip non-uniformity by about 31%. The reason can be analyzed as follows. According to the *R*-squared

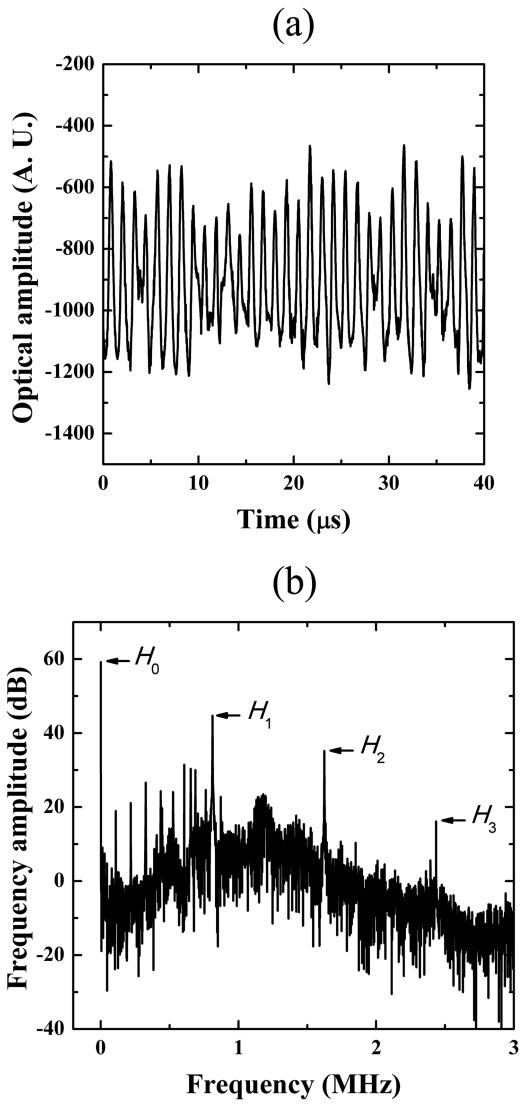

FIG. 3. (a) Optical plasma intensity variation in time domain, (b) Fast Fourier transformation data.

value analysis results in Table II, correlations $R_0^2\left(\bar{H}_{0j}, ASR\right)\approx 83.15\%$ and $R_0^2\left(\bar{H}_{0j}, SNU\right)\approx 61.20\%$ are most effective for calculating $CD_{V,j}$. Because $CD_{V,j}$ in Eq. (5) is proportional to the product of R_i^2 and $\bar{H}_{ij}$, the high values of R_i^2 and $\bar{H}_{ij}$ increase the accuracy of $CD_{V,j}$. Physically, the average photoresist strip rate is the result of a chemical reaction between the energetic gas etchants and

TABLE I. Measured harmonics intensities and wafer process results.

Inspection j	$\bar{H}_{0j}$	$\bar{H}_{1j}$	$\bar{H}_{2j}$	$\bar{H}_{3j}$	ASR[a]	SNU[b]
1	1177.713	80.803	25.886	3.192	110606	0.064
2	1325.500	91.311	28.163	2.865	115084	0.066
3	1281.138	87.616	28.491	2.795	110919	0.067
4	1413.000	83.806	25.686	2.899	117507	0.170
5	1823.625	86.749	27.853	2.793	148972	0.196
6	1351.875	88.865	26.041	2.757	115505	0.142
7	1357.250	93.474	27.220	2.730	114737	0.097
8	1370.625	92.638	25.351	2.806	116079	0.141

[a] *ASR*: Average strip rate in Å.

[b] *SNU*: Strip non-uniformity on wafer, (maximum strip rate−minimum strip rate)/*ASR*.

TABLE II. R^2 values between average harmonics intensity and wafer process results. The inspection range is $1 \le j \le 4$ in R_i^2 calculations.

Averaged harmonics intensity	$R_i^2\left(\bar{H}_{ij}, ASR\right)$	$R_i^2\left(\bar{H}_{ij}, SNU\right)$
$\bar{H}_{0j}$	83.15%	61.20%
$\bar{H}_{1j}$	5.25%	8.51%
$\bar{H}_{2j}$	7.94%	36.67%
$\bar{H}_{3j}$	13.21%	2.75%

the carbon composition on wafer. And this chemical reaction is directly proportional to the plasma electron density. As is well known in plasma physics, the rf power ($\propto \bar{H}_{0j}$) balance in reactor determines bulk plasma's electron density. However, in the case of photoresist strip non-uniformity, the lateral inhomogeneities of the plasma are more effective than the rf power balance in the reactor. Therefore, correlation $R_0^2\left(\bar{H}_{0j}, ASR\right)$ is higher than correlation $R_0^2\left(\bar{H}_{0j}, SNU\right)$, and $R_0^2\left(\bar{H}_{0j}, ASR\right)$

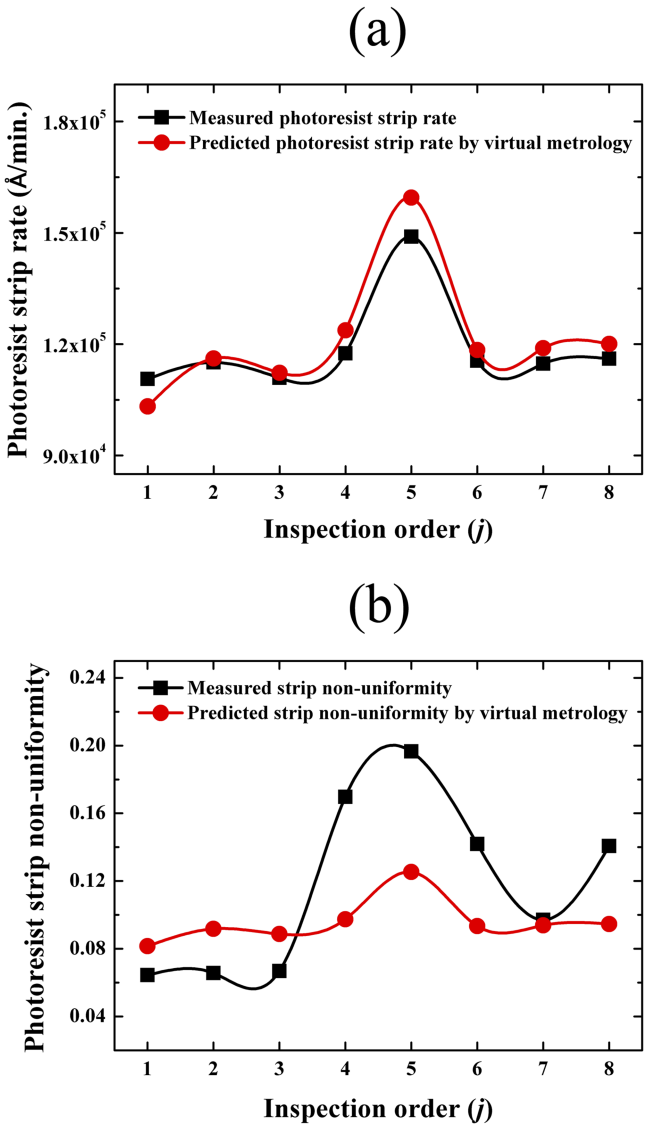

FIG. 4. Comparison of measured process results and virtual metrology results for (a) the photoresist strip rate, and (b) photoresist strip non-uniformity.

forms a higher $R^2(CD_{M,j},CD_{V,j})$ in the average photoresist strip rate. In addition to harmonics order i=0, $R_3^2\left(\bar{H}_{3j},ASR\right)$≈13.21% and $R_2^2\left(\bar{H}_{2j},SNU\right)$≈36.67% also show somewhat high levels of correlation compared to $R_i^2\left(\bar{H}_{ij},SNU\right)$ and $R_i^2\left(\bar{H}_{ij},ASR\right)$. Although measured correlations $R_i^2\left(\bar{H}_{ij},SNU\right)$ and $R_i^2\left(\bar{H}_{ij},ASR\right)$ are statistically unstable due to the small size of process inspection sample j in this experiment, we observed that correlation $R_2^2\left(\bar{H}_{2j},SNU\right)$≈36.67% is not negligible. In the current status, it can be predicted that harmonics order i=2 has coupled to lateral inhomogeneities in plasma.

The most important finding in this research is the experimental verification that plasma optical harmonics signals directly correspond with measured wafer process results. This high level of correlation can be interpreted in two ways. The first plausible reason is plasma ionization change, which is one of the key factors that determine electron density and electron temperature in plasma. It is conjectured that the variation in static optical intensity $\bar{H}_{0j}$ is proportional to the variation in bulk plasma ionization, which is directly associated with the photoresist strip rate. The fact that $\bar{H}_{0j}$ showed the highest level of correlation with the process results in our experiment supports this interpretation. The second possible reason is bulk plasma fluctuation caused by sheath modulation. Plasma harmonics signals based on the nonlinearity of the sheath are closely related to the rf phase fluctuation in electron density and electron temperature. These time-dependent changes in plasma parameters can be analyzed by the *FFT* results of the measured plasma optical intensities. Because the *FFT* results include time-dependent electrochemical reactions on the wafer surface, it is conjectured that the variation in *FFT* spectrum is proportional to the time-dependent characteristics of plasma parameters.

In addition, there are some important points to consider on the accuracy of virtual metrology. When $\bar{\alpha}$ is calculated for a relatively small size of wafer sample, such as $1\leq j\leq 4$, the short period of *CD* prediction becomes very efficient. However, because the statistical representation of $R_i^2\left(\bar{H}_{ij},CD_{M,j}\right)$ in the range of $1\leq j\leq k$ decreases, a long-term prediction of *CD* becomes inaccurate. To avoid this problem, it is necessary to update $\bar{\alpha}$ frequently. Empirically, highest *CD* predictability can be obtained when the size of the inspection group in $1\leq j\leq k$ is balanced with the size of the predicted inspection group.

V. SUMMARY

In this research, a virtual metrology technique based on plasma harmonics is developed to predict the photoresist strip process. Measured processes, such as the photoresist strip rate and strip uniformity, are statistically predicted by analyzing plasma harmonics intensities. The analytical results confirm that there is a strong correlation between the measured photoresist strip rate and optical harmonics intensities. Based on this finding, a mathematical model for predicting process results prediction is developed. The newly developed virtual metrology technique shows a 95% *R*-squared value in the photoresist strip rate, and a 64% *R*-squared value in photoresist strip non-uniformity.

Previous plasma process inspection research has been based on the analyses of plasma parameters, such as electron temperature, electron density, and electron energy probability function (*EEPF*). However, these approaches lack direct associations with the measured process critical dimension results and are not appropriate for maintaining the processes in mass production lines. Although the virtual metrology technique introduced in this study cannot show the detailed underlying physics of the plasma process, it is capable of providing numerically accurate predictions of plasma process results. Moreover, the results of our study can be applied to other semiconductor processes that use plasma. In the case of plasma dry etching, the capacitive coupled plasma process based on multiple radio frequencies is an optimum process that can measure various combinations of high-order plasma harmonics signals. As the number of measurable high-order plasma harmonics signals increases, the amount of data from plasma analysis quickly expands. These plasma harmonics signals are directly linked not only to the spatial variation in rf sheath amplitude but also to the *DC* self-bias voltage dependence of plasma parameters,[23] such as the ion energy distribution function (*IEDF*). Therefore, there will be an undiscovered physical relationship between the high-order plasma harmonics signals and the results of the dry etch process. To investigate this in the current semiconductor process, further research is necessary on the virtual metrology algorithm and the high-speed plasma optical emission sensor.

[1] J. Besnard, D. Gleispach, H. Gris, A. Ferreira, A. Roussy, C. Kernaflen, and G. Hayderer, International Journal of Control Science and Engineering **2**(3), 26 (2012).
[2] A. A. Khan, J. R. Moyne, and D. M. Tilbury, Journal of Process Control **18**, 961 (2008).
[3] S. Lynn, J. Ringwood, and N. MacGearailt, IEEE Trans. Semicond. Manuf. **25**, 94 (2011).
[4] T. Hirai and M. Kano, IEEE Trans. Semicond. Manuf. **28**, 137 (2015).
[5] J. Besnard, D. Gleispach, H. Gris, A. Ferreira, A. Roussy, C. Kernaflen, and G. Hayderer, International Journal of Control Science and Engineering **2**(3), 26 (2012).
[6] T. Hirai and M. Kano, Journal of LATEX Class Files **11**, 1 (2012).
[7] H. Purwins, B. Barak, A. Nagi, R. Engel, U. Höckele, A. Kyek, S. Cherla, B. Lenz, G. Pfeifer, and K. Weinzierl, IEEE/ASME on Mechatronics **19**, 1 (2014).
[8] C. Park and S. Kim, Journal of Process Control **42**, 51 (2016).
[9] D. Kim, P. Kang, S.-K. Lee, S. Kang, S. Doh, and S. Cho, Pattern Anal. Applic. **18**, 173 (2015).
[10] M. A. Jebri, E. M. El Adel, G. Graton, M. Ouladsine, and J. Pinaton, Journal of Physics: Conf. Series **783**, 012042 (2017).
[11] S. Park, S. Jeong, Y. Jang, S. Ryu, H.-J. Roh, and G.-H. Kim, IEEE Trans. Semicond. Manuf. **28**, 241 (2015).
[12] M. A. Lieberman and A. J. Lichtenberg, *Principles of Plasma Discharges and Materials Processing*, 2nd edition (Wiley, New Jersey, 2005).
[13] P. Chabert and N.St. J. Braithwaite, *Physics of Radio Frequency Plasmas* (Cambridge University Press, New York, 2011).
[14] S. A. Glantz, B. K. Slinker, and T. B. Neilands, *Primer of Applied Regression and Analysis of Variance*, 2nd edition (McGraw-Hill, New York, 2000).
[15] M. A. Lieberman, IEEE Transactions on Plasma Science **16**, 638 (1988).
[16] S. Rauf and M. J. Kushner, Transactions on Plasma Science **27**, 1329 (1999).
[17] V. P. T. Ku, B. M. Annaratone, and J. E. Allen, J. Appl. Phys. **84**, 6536 (1998).
[18] Y. Yamazawa, Appl. Phys. Lett. **95**, 191504 (2009).
[19] S. Wilczek, J. Trieschmann, D. Eremin, R. P. Brinkmann, J. Schulze, E. Schüngel, A. Derzsi, I. Korolov, P. Hartmann, D. Zoltán, and T. Mussenbrock, Phys. Plasmas **23**, 063514 (2016).
[20] V. Godyak, B. Alexandrovich, R. Piejak, and A. Smolyakov, Plasma Sources Sci. Technol. **9**, 541 (2000).
[21] http://www.sumcosi.com/.
[22] https://www.jawoollam.com/.
[23] A. A. Howling, L. Sansonnens, J. Ballutaud, Ch. Hollenstein, and J. P. M. Schmitt, Journal of Applied Physics **96**, 5429 (2004).